

Enhanced digital twin for on-site inspections using distributed optical fiber sensors and augmented reality

Downloaded from: https://research.chalmers.se, 2025-11-13 11:44 UTC

Citation for the original published paper (version of record):

Fernandez, I., Gil Berrocal, C., Johansson, M. et al (2026). Enhanced digital twin for on-site inspections using distributed optical fiber sensors and augmented reality. Automation in Construction, 181. http://dx.doi.org/10.1016/j.autcon.2025.106602

N.B. When citing this work, cite the original published paper.

research.chalmers.se offers the possibility of retrieving research publications produced at Chalmers University of Technology. It covers all kind of research output: articles, dissertations, conference papers, reports etc. since 2004. research.chalmers.se is administrated and maintained by Chalmers Library

ELSEVIER

Contents lists available at ScienceDirect

Automation in Construction

journal homepage: www.elsevier.com/locate/autcon



Enhanced digital twin for on-site inspections using distributed optical fiber sensors and augmented reality

Ignasi Fernandez ^{a,*}, Carlos G. Berrocal ^a, Mikael Johansson ^b, Mattias Roupe ^b, Rasmus Rempling ^{b,c}

- ^a Chalmers University of Technology, Division of Structural Engineering, Göteborg SE-41296, Sweden
- ^b Chalmers University of Technology, Division of Construction Management and Engineering, Göteborg SE-41296, Sweden
- ^c NCC Sverige AB, Sweden

ARTICLE INFO

Keywords:
Augmented reality
Distributed optic fiber sensors
Inspections
Infrastructure management
Edge computing
Enhanced visualization

ABSTRACT

Infrastructure inspections are still largely manual, episodic, and subjective, which delays damage detection and limits data-informed decision making. The paper introduces a Digital Twin framework designed to enhance infrastructure inspections using Distributed Optical Fiber Sensors (DOFS) and Augmented Reality (AR). The framework integrates advanced sensing technologies, edge computing, and web-based applications to provide real-time and historical data visualization during inspections. DOFS technology, known for its high spatial resolution and sensitivity to strain and temperature variations, is utilized to capture high-resolution strain data for continuous structural health monitoring. The framework combines DOFS data with Building Information Modelling (BIM) and AR to create a virtual representation of the assets, enabling precise and efficient on-site inspections. Two case studies demonstrate the practical application of this system: one focusing on historical data visualization and the other on real-time sensor data visualization. The results highlight the framework's ability to provide valuable insights into infrastructure health, improve inspection accuracy, and enhance decision-making processes.

1. Introduction

Most current infrastructure management strategies use time-based inspections, where an operator inspects the structure regardless of its condition and manually collects data [1]. These data are then analysed and entered in a database manually. This method has several significant drawbacks: 1) initial inspections rely purely on human visual assessment, limiting accuracy and depending heavily on the inspector's experience; 2) documentation relies on journal records and photos, making the process tedious, especially in hard-to-reach areas or adverse weather conditions, leading to inefficient data processing; 3) inspections often require partial or full closure of the infrastructure for inspector safety, which is inconvenient for users.

To enhance and support inspection processes, the monitoring of infrastructure through advanced sensing technologies such as Digital Image Correlation (DIC) and optical fiber-based strain and temperature sensors has recently been adopted in structural engineering. Optical fiber sensors offer several advantages over traditional sensors, including

their compact size, lightweight nature, and resistance to corrosion and electromagnetic interference. Among these technologies, Fiber Bragg Grating sensors are widely employed; however, their limitations in providing detailed spatial measurements render them less effective for applications such as detecting cracks in concrete. Recently, advancements in Distributed Optical Fiber Sensors (DOFS) have enabled high spatial resolution and introduced novel testing techniques. DOFS utilize light backscattering phenomena such as Raman, Brillouin, and Rayleigh scattering. The latter two are particularly pertinent to civil engineering applications due to their sensitivity to strain and temperature variations. While Brillouin-based DOFS can sense over extensive ranges of up to 300 km, Rayleigh-based systems provide superior spatial resolution, making them well-suited for detailed structural monitoring.

Distributed Optical Fiber Sensing (DOFS) is an emerging technology in structural engineering, showing potential for geotechnical and infrastructure applications [2–5]. Research indicates its capability to assess key performance indicators and monitor crack widths without strain transfer models [5,6]. When combined with advancements in

E-mail address: ignasi.fernandez@chalmers.se (I. Fernandez).

^{*} Corresponding author.

Information and Communication Technology (ICT), such as the Internet of Things (IoT), 5G networks, and wireless connectivity, along with data visualization using Building Information Models (BIM), this forms an effective approach for developing innovative structural health monitoring (SHM) systems. This integrated method is referred to as a Digital Twin (DT), which creates a virtual representation of a physical asset by merging sensor data and numerical models to simulate and visualize real-time behaviour of the asset. Typically, digital twins are used for remote monitoring; however, current infrastructure management philosophies consider on-site inspection data as crucial and complementary to sensor data [7]. Therefore, integrating the digital twin into the local environment to superimpose it onto its physical counterpart would enhance on-site inspections by providing additional practical value. Augmented Reality (AR) is identified as the most effective method to achieve this.

Augmented Reality (AR) is a technology that places computergenerated content, including graphics, text, audio, or video, onto a user's view of the real world in real time. In contrast to Virtual Reality (VR), which creates an entirely digital environment, AR enhances the physical environment by adding digital layers or annotations without completely replacing the user's surroundings [8]. The application of AR in civil engineering spans a large number of cases, from education to real life applications [9-12]. Therefore, the combination of BIM and AR results very appealing to bring visualize and represent data on the physical counterpart. Some application in this direction can be found, such as Park et al. [13] that created a defect-management workflow for civil structures by linking BIM and AR, focus on a lot on production. Another work presented by Chi et al. [14] focuses on production enhancement in the construction processes of infrastructure by allowing AR based inspection of steel reinforcement bar deployments. Zhou et al. [15] proposed an AR inspection tool for tunnels that overlays a BIM model onto the real structure using physical markers or Huang et al. [16] that built an AR visualization of finite-element results so users can see load effects in situ. More related to bridge management inspection solutions Nguyen et al. [17] implemented an integrated system based on Holo Lens device and BIM for monitoring of bridges. In more recent work by Martins et al. developed a mixed-reality framework for bridge inspection that integrates BIM models with parametric damage objects, enabling on-site visualization and damage mapping through tablets or HoloLens devices. Further, Liu et al. used drones in order to bridge accessibility issues in inspection and use still AR [18]. Melek et al. developed a realtime monitoring of cracks in concrete using AR, however, this study is limited to crack and based on image recognition pattern, not in sensor data. Despite all this work done being very advanced showing useful integrations of BIM and AR, it is difficult to find practical solutions where sensor data is brought real-time through a cloud computing infrastructure to the structure, even less when related to DOFS sensors, particularly suitable for long term monitoring of infrastructure [19]. In this regard Minghao et al. [20] introduced a system integrating DOFS and AR, however, its application is focus on pipelines and the DOFS technology based on Brillouin.

In this study, 'Digital Twin' refers to a dynamic digital replica of a physical structure, continuously updated with live sensor data DOFS and visualized through AR, providing interactive feedback for inspection and analysis. This paper introduces a simple but comprehensive digital twin concept tailored for both local and remote monitoring and inspection of infrastructure. This innovative framework employs DOFS for extensive data collection, utilizes edge computing for efficient data processing, and incorporates a web-based application for streamlined information retrieval and display. By integrating Augmented Reality (AR) for real-time data visualization and coupling with Building Information Modelling (BIM), inspectors can perform more precise, efficient, and safer inspections. The system is designed to present data in near-real time as well as historical records, providing inspectors with clear and immediate insights into infrastructure health, thereby significantly enhancing their ability to evaluate structural integrity. To demonstrate

and assess the practical application of this system, we conducted two case studies in a laboratory setting.

2. Research approach

This study adopts Design Science Research (DSR) as the overarching methodological framework. DSR is a problem-solving paradigm centred on the development of artifacts that address identified problems and deliver utility within specific application contexts [21,22]. In this approach, the artifact itself constitutes a primary outcome, along with the knowledge gained about its design, implementation, and impact within its intended environment.

The DSR process typically involves three interrelated and iterative activities: Design, Build, and Evaluate. These form the design cycle, in which alternative solutions are generated, refined, and assessed in a systematic manner. This cycle is complemented by two supporting cycles: the relevance cycle, which anchors the research in real-world needs and application contexts, and the rigor cycle, which integrates relevant theoretical and empirical knowledge from the scientific knowledge base.

In the context of this paper, the artifact developed and evaluated is a "Digital Twin system and framework for on-site inspections using DOFS. BIM and AR", designed for visualizing sensor data for informed decisionmaking during off-site and on-site inspections of infrastructures. In the current state the artifact is demonstrated and validated in laboratory setting. However, the developed technology and system aim to be applied in the end in a real-world context. Furthermore, the research not only aims to demonstrate the utility of the artifact but also to contribute insights into how and why it improves inspectors understanding, but also support more precise, efficient, and safer inspections. In the following section the Design, Build, and Evaluate process for the different system components for the Digital Twin system and framework is described. The main components are the Monitoring Component (Distributed Optical Fiber Sensors (DOFS)), the Analysis Component (cloud computing for pre-processing and analysing sensor data into "inspector datasets"), and the Interface Component (web-based application supporting intuitive retrieval and display of information using BIM and AR).

While DOFS for RC monitoring and AR for visualization have been reported, our contribution is a closed-loop, inspection-oriented Digital Twin that (i) ingests high-resolution DOFS in near real-time through a cloud/edge pipeline, (ii) derives crack onset and develoment and warps the visualization mesh using DOFS-based deflections to minimize AR misalignment, (iii) employs a simple dual-marker anchoring strategy suitable for mobile devices on site, and (iv) delivers a hardware-agnostic WebXR experience, including time-history screening and threshold-based controls. Table 1 contrasts our framework with representative prior works.

3. Digital twin framework for on-site inspections using DOFS and AR

A promising strategy to improve the understanding of the behaviour and condition of structural elements is the use of digital twins. A digital twin is a dynamic virtual replica of a physical asset that integrates numerical models with continuously updated sensor data to simulate and visualize the structure's real-time response. In this study, we propose a tailored digital twin concept specifically designed to enhance inspection workflows and support more effective asset management. The framework combines Distributed Optical Fiber Sensors (DOFS) for high-resolution data acquisition, edge computing for efficient data processing, and a web-based application for intuitive data retrieval and visualization. The system provides both near-real-time updates and access to historical records, giving inspectors clear and immediate insights into structural health and thereby improving their ability to assess integrity with greater accuracy.

The architectural framework is organized into three main

Table 1Positioning of this work against representative studies.

Study (example)	Sensor input	Real-time loop	AR alignment	Mesh/deflection warping	Hardware	Focus
Park et al. [13]	BIM + manual data	No	Marker-based	No	Tablet	Defect management workflow
Chi et al. [14]	Laser scan $+$ AR	Partial	Model-based	No	Tablet	Rebar inspection
Zhou et al. [15]	BIM overlay	No	Markers	No	Tablet	Tunnel displacement inspection
Huang et al. [16]	FE results	No	Model-based	FE only	HMD / PC	Finite element results in AR
Nguyen et al. [17]	$BIM + mixed \ reality$	Partial	HoloLens (SLAM)	No	HoloLens	Bridge inspection/maintenance
Li et al. [20]	Brillouin DOFS	Partial	Not detailed	No	Mobile device	Pipeline safety assessment
Martins et al. [33]	BIM + damage info	Partial	MR alignment (SLAM + BIM parametric objects)	No	Tablet / HoloLens	Bridge inspection (damage mapping with BIM)
This work	Rayleigh DOFS (mm- scale)	Yes (<10 s)	Dual QR markers	Yes (DOFS-based)	WebXR (mobile)	On-site inspection digital twin

components: the Monitoring Component, the Analysis Component, and the Interface Component. Their interconnections and distinct roles are illustrated schematically in Fig. 1, offering an overview of how the system operates as an integrated whole. Each component is described in detail in the following sections.

3.1. Data monitoring

The infrastructure monitoring system includes all components required to measure the physical response of the structure: the sensors, the interrogator, and the devices enabling remote data access (gateway or router and server). All monitoring hardware must be installed on site at the structure being assessed. In this study, an Optical Distributed

Sensor Interrogator (ODiSI 6000 series, Luna Inc.) was used. The interrogator was configured with a spatial resolution of 2.65 mm between measurement points and a sampling rate of 1 Hz. For sensing, the BRUsens V9 cable (Solifos) was employed in both case studies. This cable, with its inner steel tube and rugged polyamide cladding, is mechanically robust, easy to handle, and well suited for embedding in reinforced concrete elements without risk of rupture.

The monitoring module maintains a secure TCP/IP connection with the ODiSI interrogator, enabling continuous data streaming at the defined sampling rate. Sensor data are buffered locally to prevent loss during slower retrieval periods, with the buffer cleared once the connection is terminated. The retrieved data are then stored and passed to the analysis module for post-processing.

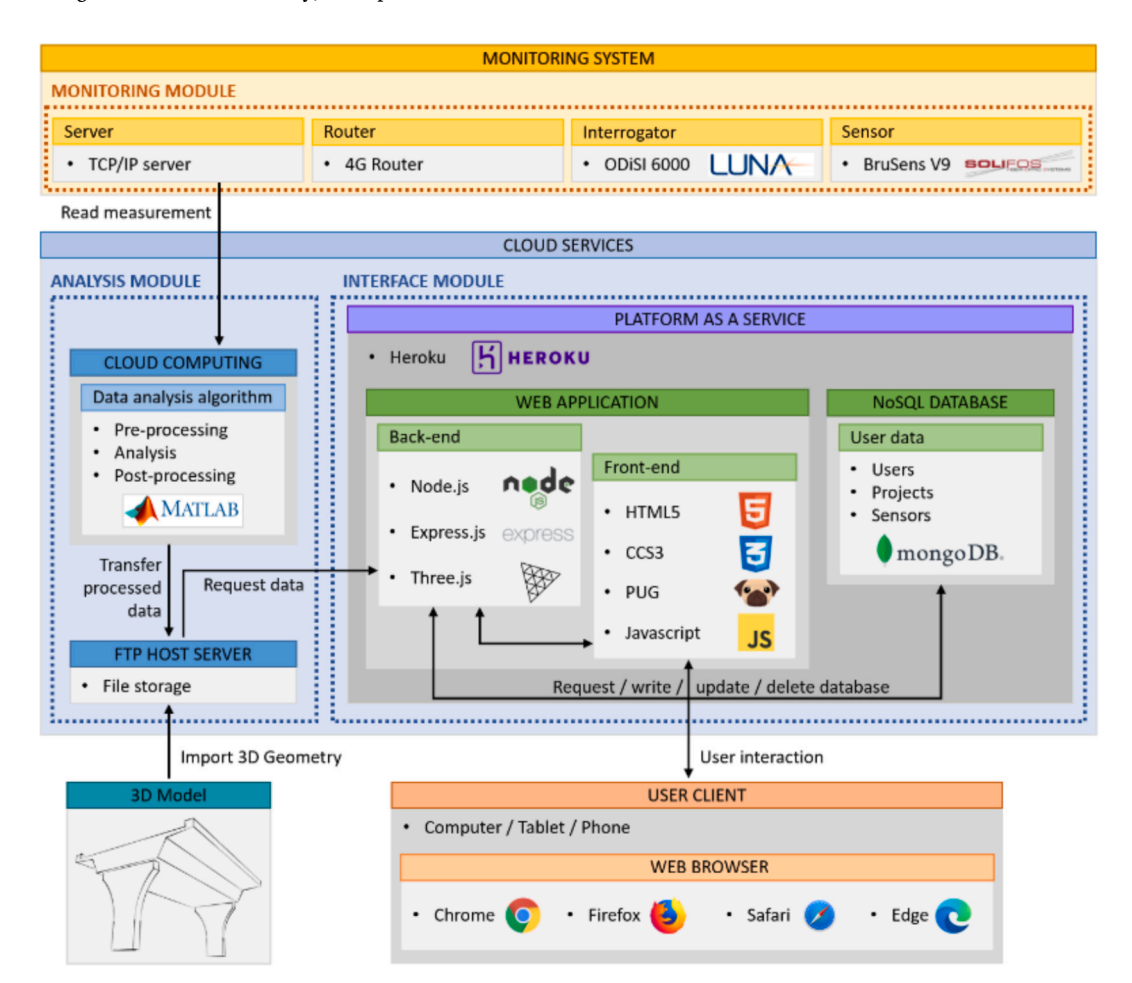


Fig. 1. Schematic representation of the web-based asset inspection system's architecture.

3.2. Analysis of sensor data

This section details the specially developed algorithms for preprocessing and analysing sensor data received through the API from the monitoring component. Subsequently, both pre-processed and postprocessed data are transmitted to and stored in a database. From there, data can be served to external clients on demand via a secondary API described below.

It must be noted that the direct readings of the strain data acquired through OFDR-based DOFS were filtered using spike removal routines, with additional moving-window regularization beyond the 2.65 mm spatial resolution to reduce noise while preserving strain gradients. The armoured cable used (BRUsens V9, Solifos) further enhanced measurement stability by limiting local distortions on the readings due to the presence of aggregates and pores in the concrete.

3.2.1. Crack detection

Previous literature has highlighted that strain measurements from Distributed Optical Fiber Sensors (DOFS) cables enables the detection of crack initiation and propagation with significant accuracy. Additionally, Berrocal et al. [6] have demonstrated that strain profiles closely align with Digital Image Correlation (DIC) measurements, as illustrated in Fig. 2. From these studies it can be concluded that DOFS facilitates the detection of crack onset at a considerably earlier stage compared to solutions based on DIC.

The analysis of strain measurements from the tensioned steel reinforcement bar served as input for a crack detection subroutine within the analysis component, aimed at identifying crack initiation in real time. A significant challenge in identifying potential crack candidates involves establishing a threshold within the measurements that distinguishes whether a detected peak indeed corresponds to a crack, as depicted in Fig. 2. In relation to crack detection, several aspects should be considered. First, cracks may occasionally cause local data loss due to the sharp strain gradients that develop at their location. This effect is mitigated by the use of robust sensing cables, which laminates the strain transfer to neighbouring measurement points. Second, the apparent smoothing visible in the figures reflects as well, interpolation for visualization purposes and does not represent a loss of physical detail in the underlying measurements. Finally, since the framework focuses on performance indicators such as crack widths and deflections, both derived from integrated strain fields over longer regions, the accuracy of these indicators is not affected by such local smoothing or loss of data.

In this study, peak prominence was selected as the criterion for identifying potential cracks, as illustrated in Fig. 2 – Detail 1. The evaluation procedure was as follows.

 A reference prominence value was defined, above which a peak was considered indicative of a crack. For this work, a threshold of 8

- microstrains was adopted. While this value may vary slightly depending on the geometry of the specimen, its variability is limited to only a few microstrains across different structures. This threshold is relevant mainly for the early detection of cracking and does not affect the subsequent accuracy of crack width or crack location measurements.
- Based on the input data, a calculated prominence value was then derived, equal to 5 % of the maximum strain recorded by the sensor. Since prominence generally increases with load level, this ensured sensitivity across the loading history.
- 3. If the calculated prominence fell between 2 and 8 microstrains, it was used directly to identify crack candidates. For values below 2, a fixed prominence of 2 was applied to reduce false positives, while for values above 8, the threshold was capped at 8 to ensure incipient cracks were not overlooked.

This adaptive approach highlights both the complexity of reliable crack detection and the importance of a calibrated threshold that responds to varying conditions and structural geometries.

3.2.2. Crack width

In this study, the methodology for calculating the crack widths of identified crack candidates follows the simplified approach outlined by Fernandez et al. [5]. As detailed in their previous work, the contribution of the concrete to the crack width calculation is disregarded, leading to the determination of crack width through the integration of $\varepsilon^{DOFS}(x)$ over the specified length, namely the distance between the preceding and following valleys. This method presumes the strain measured corresponds directly to the strain in the steel, see Eq. 1.

$$\mathbf{w}_{cr,i} = \int_{-l_{r,i}}^{t_{r,i}^{+}} \varepsilon^{DOFS}(\mathbf{x}) d\mathbf{x}$$
 (1)

This simplification should yield reasonable results and an upper limit of the crack width, being the actual crack width equal or smaller, depending on the real contribution of the surrounding concrete.

3.2.3. Curvatures, rotations, and deflections

The methodology employed in this study to compute the beam deflections under a specific load level adopts the framework introduced by Berrocal et al. [6], utilizing the principles of Euler-Bernoulli beam theory. This theory presupposes that beam sections under load maintain planarity within the deformation plane, meaning all strains across a cross-section are orthogonal to it, and overlooks shear deformation contributions. Accordingly, the beam deflection, $\nu(x)$, is governed by the Eq. 2.

$$\frac{M(x)}{EI} = -\frac{d^2v(x)}{dv^2}$$
 (2)

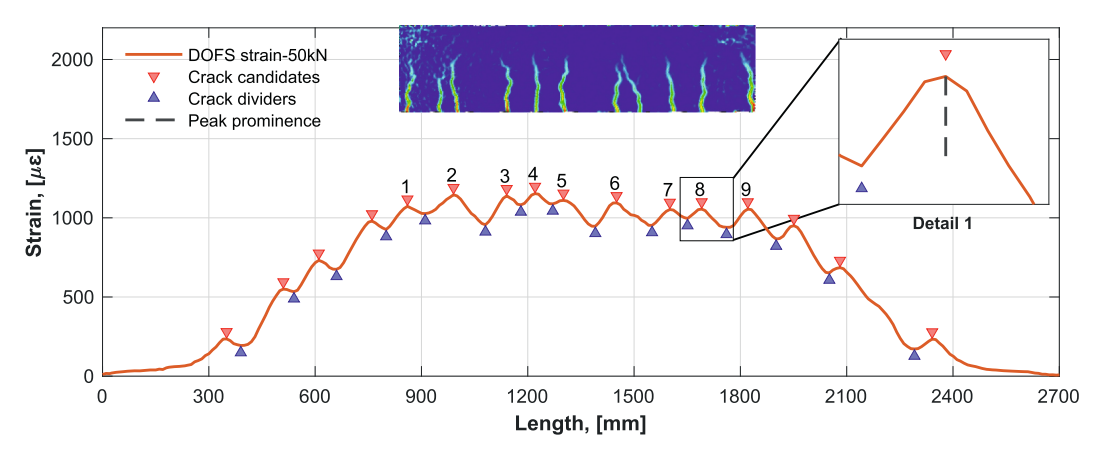


Fig. 2. Crack detection from DOFS sensors compared to DIC measurements [23].

where M(x) is the bending moment distribution and EI is the flexural stiffness of the section.

Several methods exist for reconstructing rotations and deflections from strain data, including modal transformation methods and inverse finite element methods. In this work, an integration-based approach was chosen because it directly exploits the distributed nature of DOFS measurements, requires no prior knowledge of modal properties or detailed finite element models, and remains computationally lightweight for near-real-time evaluations. While numerical integration may accumulate errors along the measurement length, for service-state conditions, where curvatures vary smoothly, this approach has been shown to provide sufficiently accurate results for inspection purposes. Furtehrmore, this is the most natural and simple approach for elements where beam theory is applicable.

Assuming that section rotation is very small, the ratio M(x)/EI can be expressed as the curvature of the beam $\chi(x)$ at any point of the beam, which can be determined as the change of normal strain per unit length across the beam's height. Consequently, the curvature is calculated based on the difference between the strains measured by two DOFS located at two different known heights, see Fig. 3, specifically at the top and bottom rebars, see Eq. 3.

$$\chi(x) = \frac{\varepsilon_{bot}(x) - \varepsilon_{top}(x)}{f_{dist}}$$
 (3)

where f_{dist} denotes the vertical distance between the DOFS cables. By determining the curvature distribution, both rotations and deflections can be derived through direct integration of the curvatures once and twice, respectively. Application of two known boundary conditions facilitates the determination of the integration constants.

Illustrated in Fig. 4 is the curvature, rotation, and deflection distribution along a beam subjected to a typical symmetric four-point bending setup. This beam is simply supported at both ends. The curvature distribution's profile closely mirrors the strain pattern, where curvature peaks similarly denote crack locations, highlighting the localized reduction in flexural stiffness at these cracked sections. The depicted slopes and deflections conform to the antisymmetric and symmetric distributions expected from the applied loads and boundary conditions, respectively.

In the targeted service state, concrete and steel behave predominantly elastically and bond between steel and concrete is very good, which means that plane-section remain a good approximation. At a crack, the DOFS attached to the tension reinforcement provides a direct approximation of the steel strain, while the compression-zone DOFS tracks the concrete compressive strain. Hence, the curvature definition in Eq. (3) remains valid at cracked sections because it is based on the measured strain gradient across the depth rather than on an intact bottom concrete fiber. Between cracks, tension stiffening reduces the bottom strain; however, the strain difference over the known lever arm still represents the effective curvature. Further, cracked section curvatures governs integrated rotations and deflections at service loads. This

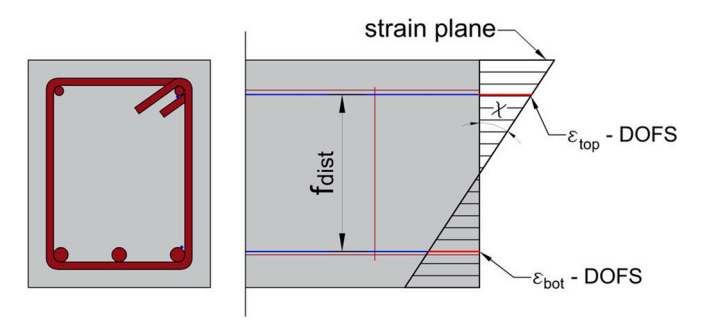
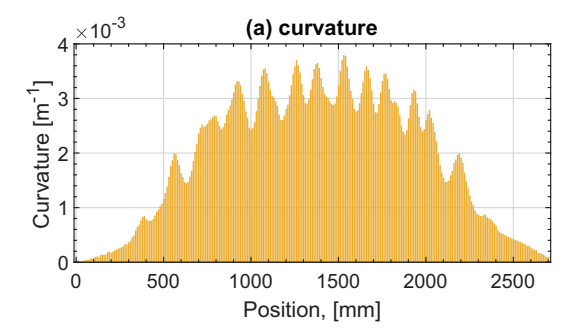
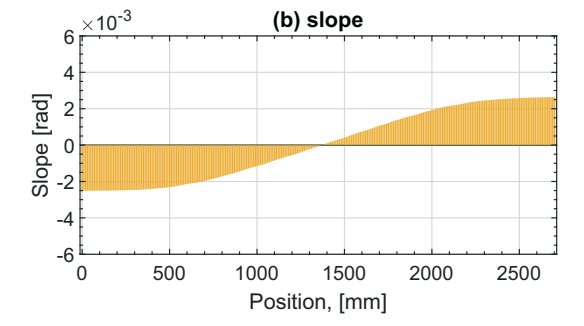


Fig. 3. Euler-Bernoulli theory, plane deformation of the cross-section in beams subjected to dominant bending.





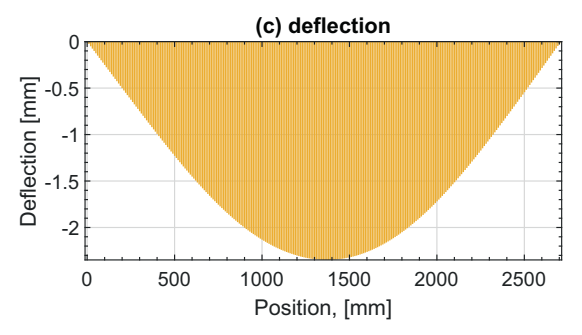


Fig. 4. Result of computing distributed (a) curvatures, (b) slopes and (c) deflections.

study therefore restricts deformation reconstruction to service-state conditions.

3.3. Post-processing data for visualization

This section elaborates on the methodology employed for post-processing Distributed Optical Fiber Sensor (DOFS) data for visualization as contour plots overlaid on the beam geometry.

3.3.1. Geometry update

The beam's spatial domain, shown in Fig. 5(a), was discretized into a uniform grid covering the entire concrete surface Fig. 5(b). The strain data obtained from the DOFS cables were then extrapolated onto these grid points. To facilitate communication between the pre-processing, post-processing, and visualization modules, the grid was transformed into a mesh of interconnected elements. In the unloaded state, this mesh was generated using the Delaunay triangulation method, producing a uniform set of triangular elements Fig. 5(c). The procedure yields three matrices that define the mesh: node identifiers, nodal coordinates, and element connectivity.

The nodes from the interconnected elements facilitate the construction of various surface plots, with the node coordinates (X, Y, and Z) indicating their spatial positions within the beam. The contour plots are determined by the matrix C, which holds the data values to be visualized. The visualization of the data is done by the interpolation of the node's values, and a color is assigned depending on the max and min values within the C matrix, see Fig. 6. A notable challenge in overlaying

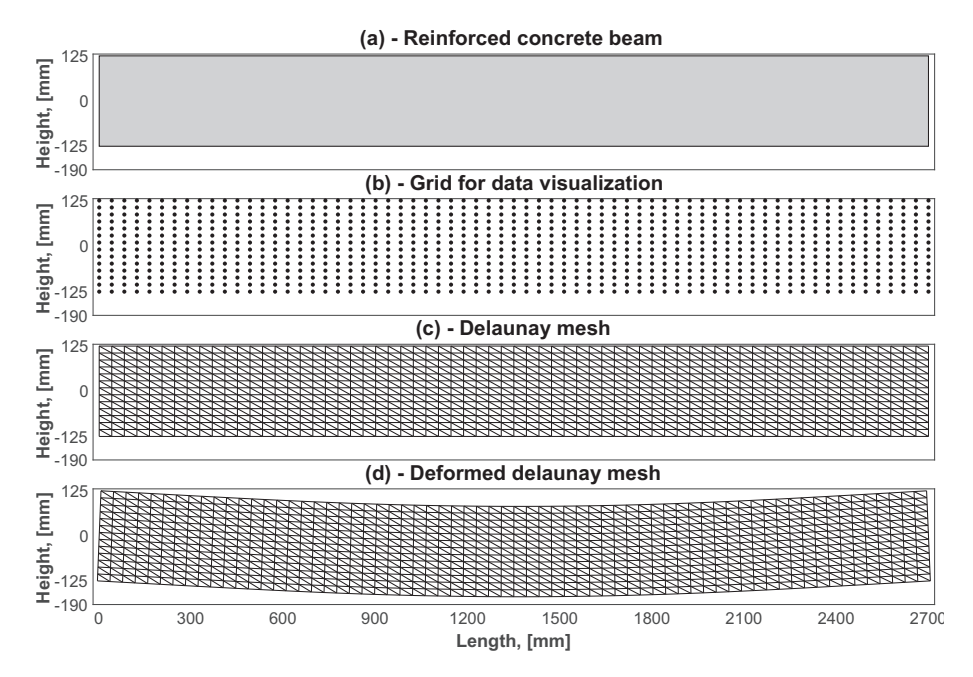


Fig. 5. Mesh obtention process and mesh deformation according to the recorded strains for data visualization. (a) Original undeformed beam, (b) initial discretization of the beam in a regular grid (plotting points), (c) mesh for data visualization based on the regular grid and (d) deformed shape of the mesh from DOFS data.

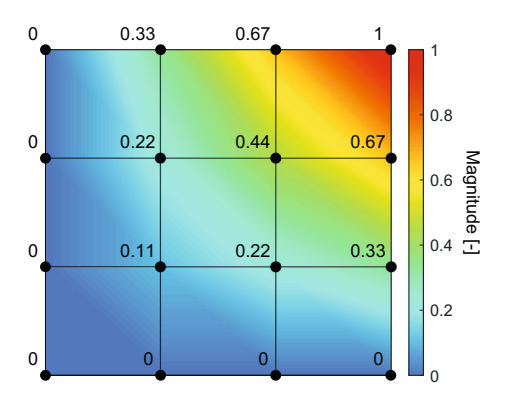


Fig. 6. Interpolation of node values for the data visualization in contour plots.

surface plots onto the beam is the discrepancy caused by beam deformation under load, making the contour plots and the deformed beam increasingly divergent with rising load levels. To address this misalignment and enhance data visualization accuracy, the mesh, as

shown in Fig. 5(c), is adjusted to reflect the actual beam deflections.

As detailed previously, deflections are computed following Euler-Bernoulli beam theory, which allows for the determination of each element's coordinate changes assuming a plane deformation. Given the rotation of a section under external load, both longitudinal and vertical displacements for each point along the section's height can be calculated, see Eq. (4) and (5) respectively.

$$X_{n,i} = x_{n,i} - \Delta u = x_{n,i} - \sin(\varphi(x_{n,i})) \cdot y_{n,i}$$
(4)

$$Y_{n,i} = \nu(x_{n,i}) + \Delta \nu = \nu(x_{n,i}) + \cos(\varphi(x_{n,i})) \cdot y_{n,i}$$
(5)

Where $x_{n,i}$ and $y_{n,i}$ are the original node coordinates, with v and φ representing deflection and rotation, respectively, derived from the reference value at the neutral axis for the given position $x_{n,i}$, as shown in Fig. 7.

After applying the described transformation to the nodes' coordinates a new representation of the mesh is obtained, which means that the new mesh position matches the deformation of the beam, see Fig. 5(d). It must be noted that this approach retains the original mesh structure, including the connections and node identifiers, across all loading steps. The later, significantly simplifies the post-processing

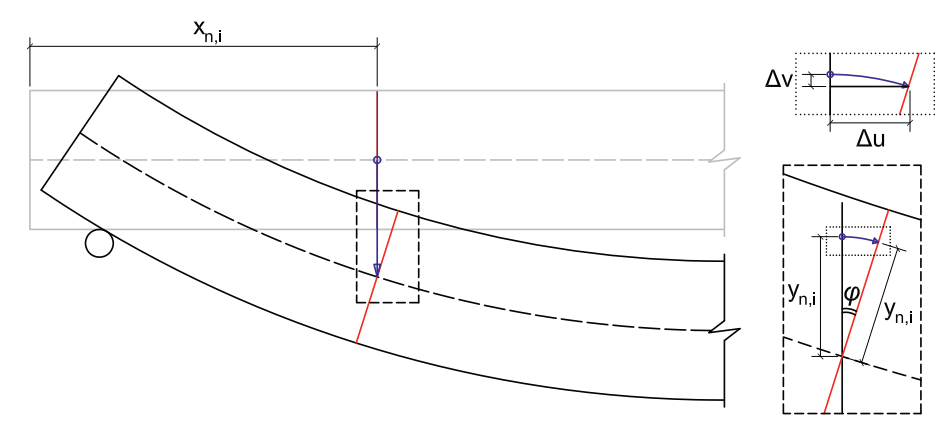


Fig. 7. Vertical and horizontal displacements obtained from the beam's neutral axis deflection calculated by Euler-Bernoulli theory.

process allowing contour plot values to be calculated using the original mesh, with positions updated separately and independently.

3.3.2. Strains, crack pattern and deflections

The strain data obtained from the DOFS cables situated at the corresponding steel reinforcement bars, Fig. 8(a), are directly extrapolated based on the hypothesis of plain deformation plane. This assumption is valid for the beam specimens studied here, where plane deformation

sections are preserved, and ensures accurate reconstruction of deformations. For structural elements where this assumption does not hold, such as slabs with non-uniform strain distributions, alternative methods are required. For example, Fernández et al. [2] demonstrated how DOFS measurements can be extrapolated to reconstruct principal strain fields in slab elements.

Consistent with this hypothesis the neutral axis of the cross-section, i. e. the point where a null value of the strain is obtained and the strain

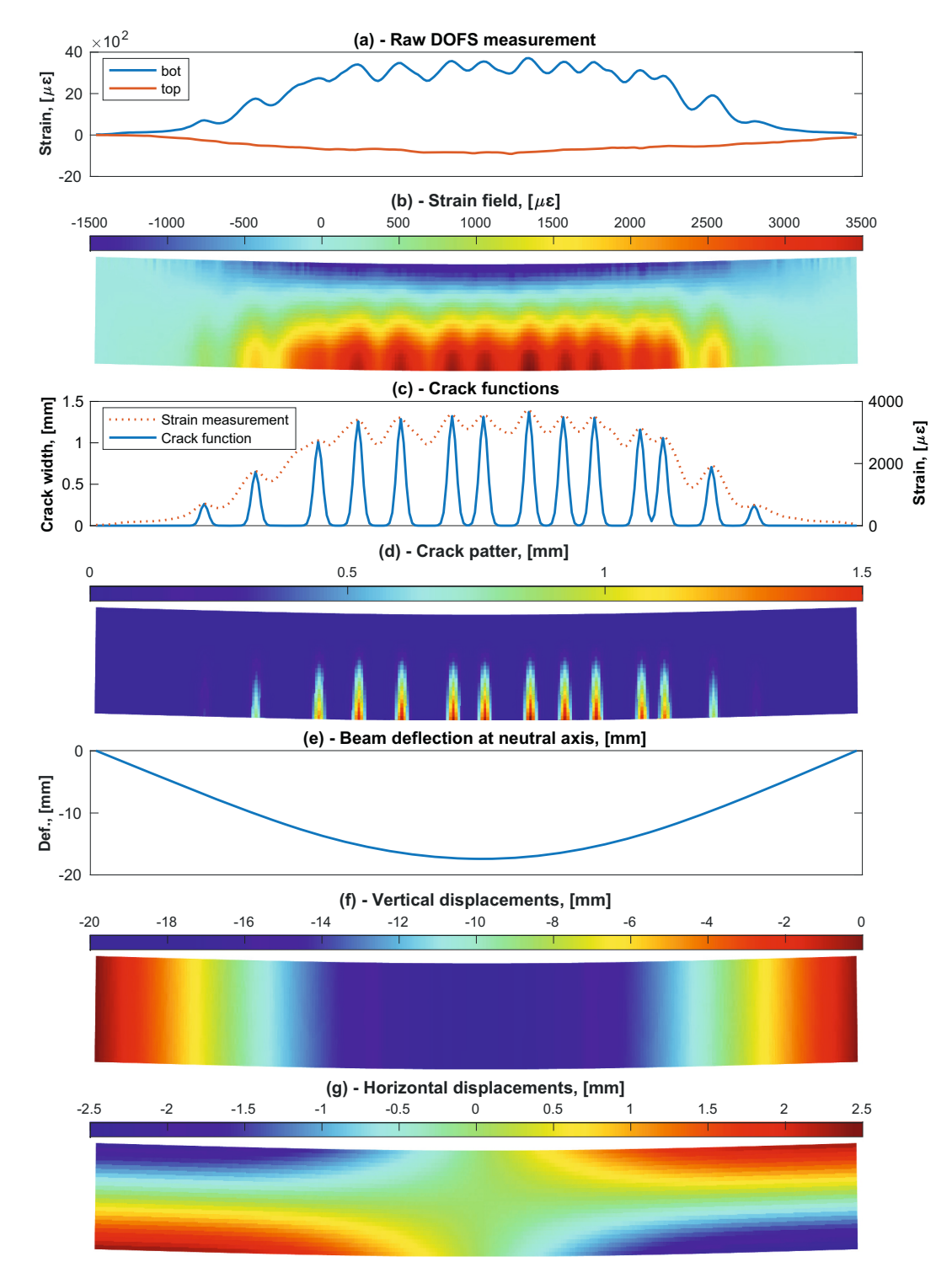


Fig. 8. (a) DOFS strain data, (b) extrapolated strain field on the concrete surface from the DOFS data, (c) outcome of the crack detection module from DOFS measurements and corresponding crack functions for data visualization, (d) crack visualization extrapolated from the crack function, (e) calculated beam deflection from the DOFS data at the beam's neutral axis, (f) and (g) Vertical and horizontal displacements computed from the beam deflection at the neutral axis.

value at any height of the cross-section can be computed according to Eq. (6).

$$\varepsilon_{\gamma}(\mathbf{x}_{n,i}) = \chi(\mathbf{x}_{n,i}) \cdot \mathbf{y}_{n,i} \tag{6}$$

Where χ denotes the curvature calculated according to Eq. (3), and x and y are the coordinates of the nodes. This data, once calculated at each mesh node, facilitates visualization as a contour plot on the beam's deformed shape, as illustrated in Fig. 8(b).

Visualization of the crack pattern through contour plots leverages the identified crack candidates. Following the detection of crack candidates, strain data undergo further post-processing to visualize both the cracks and their respective widths. In order to obtain a better visualization of the cracks and a more robust algorithm to post-process the data, the method presented by Berrocal et al. [6] is further developed. The present algorithm utilizes the same approach to transform the strain measured by the cables to crack values, i.e. crack functions are generated to create crack profiles that can be suitable for visualization purposes. In this regard, the crack functions are generated for each crack using a gaussian curve with a peak value equal to the computed crack width and a width of 4 cm.

For a refined representation, each mesh node is initially assigned a crack width of zero. Where a crack is identified by the detection algorithm, linear extrapolation along the nodes within the cross-section height is executed. This extrapolation process includes calculating crack width at varying heights reinforcement level, one-third and two-thirds of the crack height, the neutral axis (where the crack fully closes), and the top reinforcement position assuming a linear closure from the section's bottom to its neutral axis, beyond which it remains closed. A typical crack pattern using the developed algorithm is illustrated in Fig. 8(d).

Lastly the displacements are simply calculated as the difference between the new calculated vertical position of the mesh nodes, according to Eq. (4) and (5), and the original vertical position of the node, as described in the Eq. (7) and (8).

$$\delta_{n,i}^{\mathbf{x}} = X_{n,i} - X_{n,i} \tag{7}$$

$$\delta_{n,i}^{\mathsf{y}} = Y_{n,i} - y_{n,i} \tag{8}$$

Where $X_{n,i}$ and $Y_{n,i}$ are the new horizontal and vertical node's coordinate and $x_{n,i}$ and $y_{n,i}$ the original horizontal and vertical position of the nodes, respectively. Fig. 8(f) and Fig. 8(g) display the horizontal and vertical deflection visualization for a specified load step, illustrating the method's capacity to accurately represent structural deformations.

3.4. Data retrieving and uploading to cloud-services API

An application programming interface (API) was developed and integrated into the system architecture to act as a communication bridge between the monitoring module, the analysis component, and the cloud services. Implemented in Python, the API periodically queried the monitoring module for new sensor data and then awaited a trigger from the calculation module, activated once all processing tasks and data files had been generated. Upon activation, the API uploaded the relevant data—tagged with identifiers such as data type (e.g., deflections, cracks, strains), measurement units, timestamp, and group identifier—to a cloud-based, non-structured database hosted on the Azure® infrastructure. Although a structured database could have been employed for time-series data, the selected setup proved effective for this study.

The frequency of API calls was defined by the minimum time required for each system component to complete its tasks, including data retrieval (influenced by data volume and internet speed), analysis (conversion of strain data into inspection parameters), and post-processing (preparation of results for AR visualization). In the presented applications, this workflow typically completed in less than 10 s, allowing near real-time visualization of structural response. For larger

structures, where data volume and computational demand are higher, the API call interval may need to be extended. Furthermore, the reading interval is dynamically adjusted based on the available on-site internet connectivity.

3.5. Client communication API

The client communication API, hosted on the cloud-based service servers, continuously listened for incoming requests, thereby establishing direct connections between client devices and the servers storing the post-processed data. Data retrieval requests relied on two identifiers: a time value and a data type. If the exact timestamp was unavailable, the system automatically returned the closest available time step.

This setup proved highly efficient and robust for time-history evaluations, where complete datasets must be accessed and reviewed. However, it is less efficient for real-time evaluation, as the client sends periodic requests regardless of whether new data are available. In such cases, redundant transfers occur because the most recent time step is repeatedly retrieved even when no new data exist.

To address this, two alternative communication strategies have been considered:

- An uncoupled channel (computational module → cloud storage → client), well-suited for time-history analysis, as implemented in the present framework.
- A direct channel (computational module → client), better suited for real-time monitoring, as it enables the client to update only when new data become available.

The second approach has clear advantages for real-time inspection, but it also raises security concerns, since mobile clients currently support only secure, certified connections. While this limitation poses a challenge during the present development stage, it is not expected to hinder future large-scale implementations, where certified secure connections between modules and clients can be more readily ensured.

3.6. Data visualization through AR

Augmented Reality (AR) solutions have gathered significant interest in recent years due to their adaptability in displaying sensor data from extensively utilized Building Information Modelling (BIM) models. The proliferation of these solutions is supported by specialized hardware and the arrival of sophisticated AR frameworks for mobile devices, such as ARKit (Apple) and ARCore (Google). These platforms leverage camerabased Simultaneous Localization and Mapping (SLAM) algorithms to construct a simplified internal 3D representation of the surroundings, enabling the placement of virtual objects within it. A notable effort has been made to democratize the application of this technology through the introduction of WebXR, a web-based AR framework. WebXR facilitates the development of software and hardware agnostic solutions with unified source code, further supporting the use of ubiquitous opensource web development libraries.

An essential challenge in AR tool development is the precise alignment between the real-world environment, captured by the device's cameras, and the superimposed virtual objects. Although various methods exist, this project employs a marker-based approach, which hinges on anchors, image and marker tracking, and alignment.

WebXR, like modern AR systems, employs SLAM to forge an internal 3D environmental representation, enhancing object positioning accuracy over time. This necessitates the anchoring of virtual objects to real-world counterparts to maintain their relative positions despite global spatial changes. Anchors allow virtual objects to update their positions dynamically in relation to physical locations, significantly mitigating discrepancies such as "floating" objects. Thus, the relation between physical and virtual object is prioritized in front of absolute positions in the space.

Additionally, WebXR's image tracking capabilities enable the recognition of general images or specific markers, such as QR codes, which are easily recognizable due to its unique patterns and high contrast. Registered images, once detected within a session, are assigned real-world coordinates, facilitating the alignment of virtual to real objects. The integration of anchoring with this tracking mechanism ensures that virtual objects not only adopt the local coordinate system of the markers but are also anchored to the physical environment, enhancing alignment accuracy, as demonstrated in Fig. 9.

To refine the alignment of post-processed sensor data with the actual beam, a dual-marker system is implemented. This approach minimizes deviations in data overlay, especially for larger objects, by defining a unique local coordinate system from the markers' centers, anchored to the beam. The sensor data's rendering coordinate system is positioned midway between the markers, independent of their rotations, as detailed in Fig. 10.

Finally, a user interface (UI) is crucial for rendering the specific data via WebXR. WebXR offers the capability to employ standard web development tools such as Hypertext Markup Language (HTML) and Cascading Style Sheets (CSS) for crafting and styling the web interface and leverages the Three.js library for efficient contour plot visualization, based on open-source graphic library OpenGL. By combining HTMLbased WebXR for AR with QR codes that serve both as spatial trackers and link to a webpage (URL carriers), the framework enables identification of the infrastructure under inspection. This user interface supports on-site inspections by detecting and spatial positioning the relevant infrastructure and loading the corresponding AR scene automatically. Furthermore, the interface facilitates data display (e.g., strains, cracks, deflections) and allows dynamic scaling of contour plots based on user defined min and max values. A time-history module enables data screening over time through a slider, adjusted for min and max timestamp values. For real-time sensor data, an open database connection updates the AR system with the latest data, considering the operational time required for data fetching, processing, and storage. An illustration of the interface, showcasing its functionalities, is presented in Fig. 11.

4. Results: Case studies

In order to illustrate the capabilities of an AR solution for enhanced inspection of infrastructure two case studies are presented in the following.

4.1. Case study 1: Visualization of historical data

For the visualization of historical data, data retrieved from Distributed Optical Fiber Sensors (DOFS) during the pre-cracking test of a large-scale reinforced concrete beam was utilized. Fig. 12 provides a comprehensive overview of the beam's geometry, the arrangement of sensors, and the testing setup. The beam underwent testing within a conventional four-point bending configuration, with the boundary conditions being that of simple supports. The load was symmetrically applied across the beam via a distribution beam, ensuring uniform loading conditions. The loading process involved three cycles of

monotonic ascending/descending ramps, regulated by the jack's local displacement.

Fig. 13(a-b) presents the measured strain at the bottom bar during the initial loading phases. As depicted in Fig. 13(a), the implemented crack detection algorithm successfully identified the first crack at an early stage of loading. Subsequent load increments resulted in additional cracks, which were also detected by the same algorithm. Fig. 13(c) displays the calculated deflections, determined using the methodology outlined in Section 3.2.3, corresponding to each load step. These deflection values are subsequently utilized in further analyses to compute mesh deformation, enabling representation of the beam's deformed shape and facilitating data visualization on the deformed mesh. Further experimental measurements for case study 1 are presented in [6].

A dual-marker solution was implemented for alignment purposes, entailing the attachment of two QR code markers to the beam's surface as depicted in Fig. 14. These markers, defined as anchors within the AR system to the beam's geometry, were strategically placed at the beam's ends to minimize potential rotation issues of the overlaid information. Accordingly, the centre of each marker was positioned 125 mm from the top and beam-end on both sides, with the data rendering's local coordinate system cantered on the beam.

Fig. 15 showcases an example of the data visualization. It is important to note that within the time history module, the data is overlaid on the structure in its unloaded form, as per the generated mesh displayed in Fig. 5(c). This approach aims to avoid misalignment between the overlaid data and the beam, which could potentially confuse or mislead the user. Nevertheless, the implementation of a toggle feature could allow users to choose between visualizing the data on deformed or undeformed meshes for enhanced flexibility. To provide a clearer understanding of the entire process, including the alignment through marker tracking and data visualization, a comprehensive video encompassing all steps is available at the provided link.

4.2. Case study 2: Real-time visualization of sensor data

To demonstrate the effectiveness of the real-time crack detection module in practical scenarios, a second case study was conducted through a live demonstration test, using a full-scale post-tensioned reinforced concrete beam. The geometric details, sensor arrangement, and testing setup are depicted in Fig. 16. This beam was subjected to the same testing configuration as the previous case study, but with the load monotonically increased until failure.

Fig. 17(a-b) presents the same results shown in Fig. 13, but for the Posttensioned Reinforced beam instead. As seen in Fig. 17(a-b), the implemented crack detection algorithm properly identifies the crack at a very early stage. Subsequent load increments resulted in additional cracks, which were also detected as well. The deflections of the beams for the different load steps shown in the Fig. 17(a-b) are depicted in Fig. 17(c). Further experimental measurements for case study 1 are presented in [24].

For this experiment, a two-marker strategy was also utilized, with markers positioned approximately 7.5 m apart. Markers were affixed to the interior of the beam's web, and the central point of the beam was





Fig. 9. Example of marker-based AR to aid positioning of virtual objects.

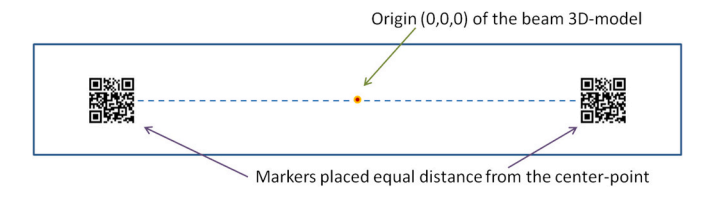


Fig. 10. Definition of the AR's global coordinate systems based on markers for data visualization.

designated as the origin of the local coordinate system. Fig. 18(a) displays the location of the left marker.

Upon detection of both markers and successful establishment of the new local coordinate system, the AR component presents an initial virtual object, a BIM model of the beam. This model outlines the external concrete geometry with a wireframe along the beam edges and provides intricate details of the reinforcement bars and sensor cables, as shown in Fig. 18(a-b). Visualizing the steel reinforcement overlaying the concrete geometry offers valuable insights into the structural behaviour under

load, enhancing understanding beyond what traditional drawings can provide. This model remains visible until the communication API is activated, and sensor data begin to be received by the device.

With the first data request through the API, the BIM model is hidden, activating the data visualization environment. Fig. 19(a) reveals the crack pattern at an incipient stage, showcasing the crack detection module's ability to operate in real-time. Cracks identified by the AR system, imperceptible to the naked eye due to their minuscule size, underscore the effectiveness of DOFS in early crack detection and its

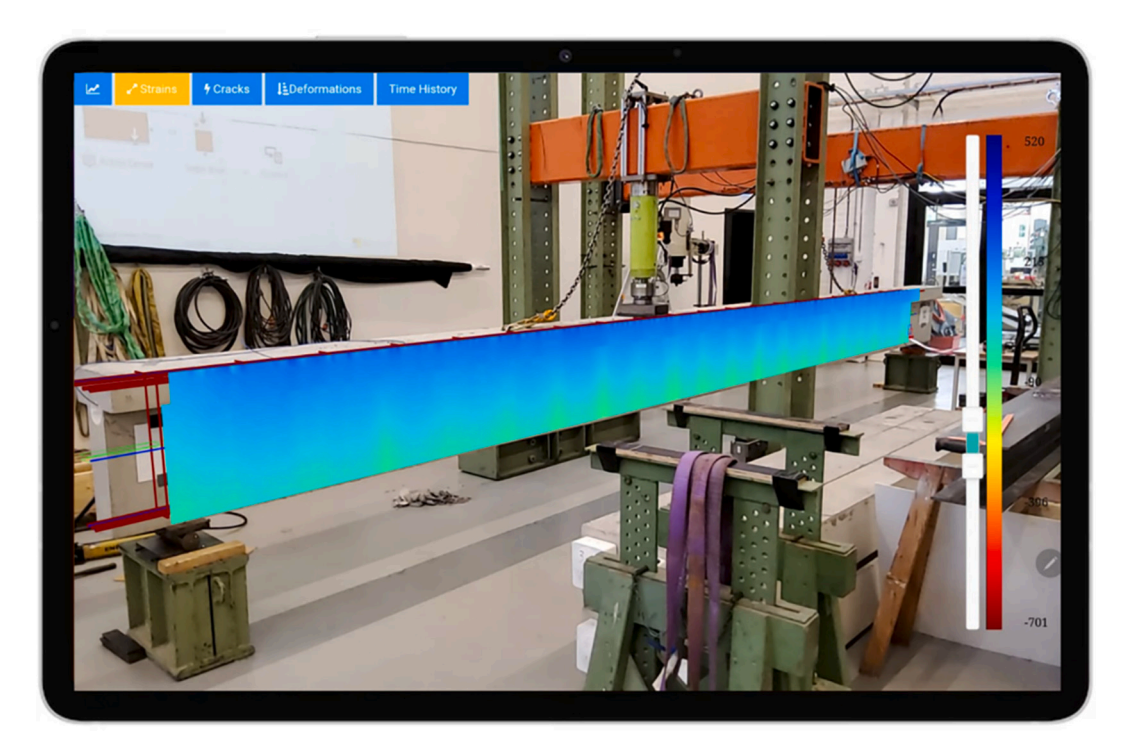


Fig. 11. Web based interface to interact with the backend and data analysis module, and data visualization.

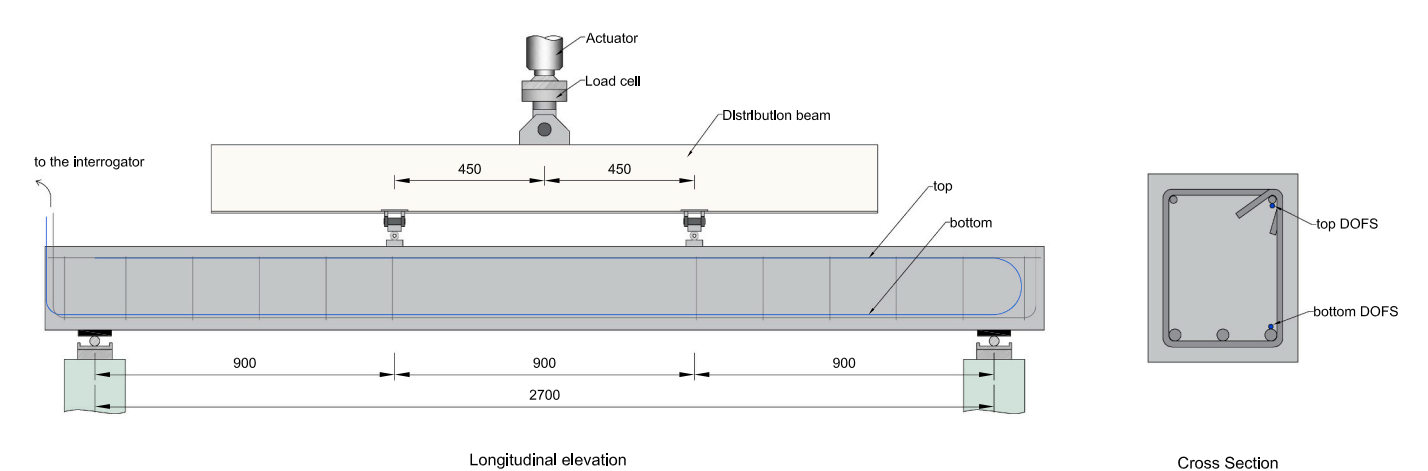


Fig. 12. Geometry, loading setup and DOFS installation configuration for the RC beam specimen.

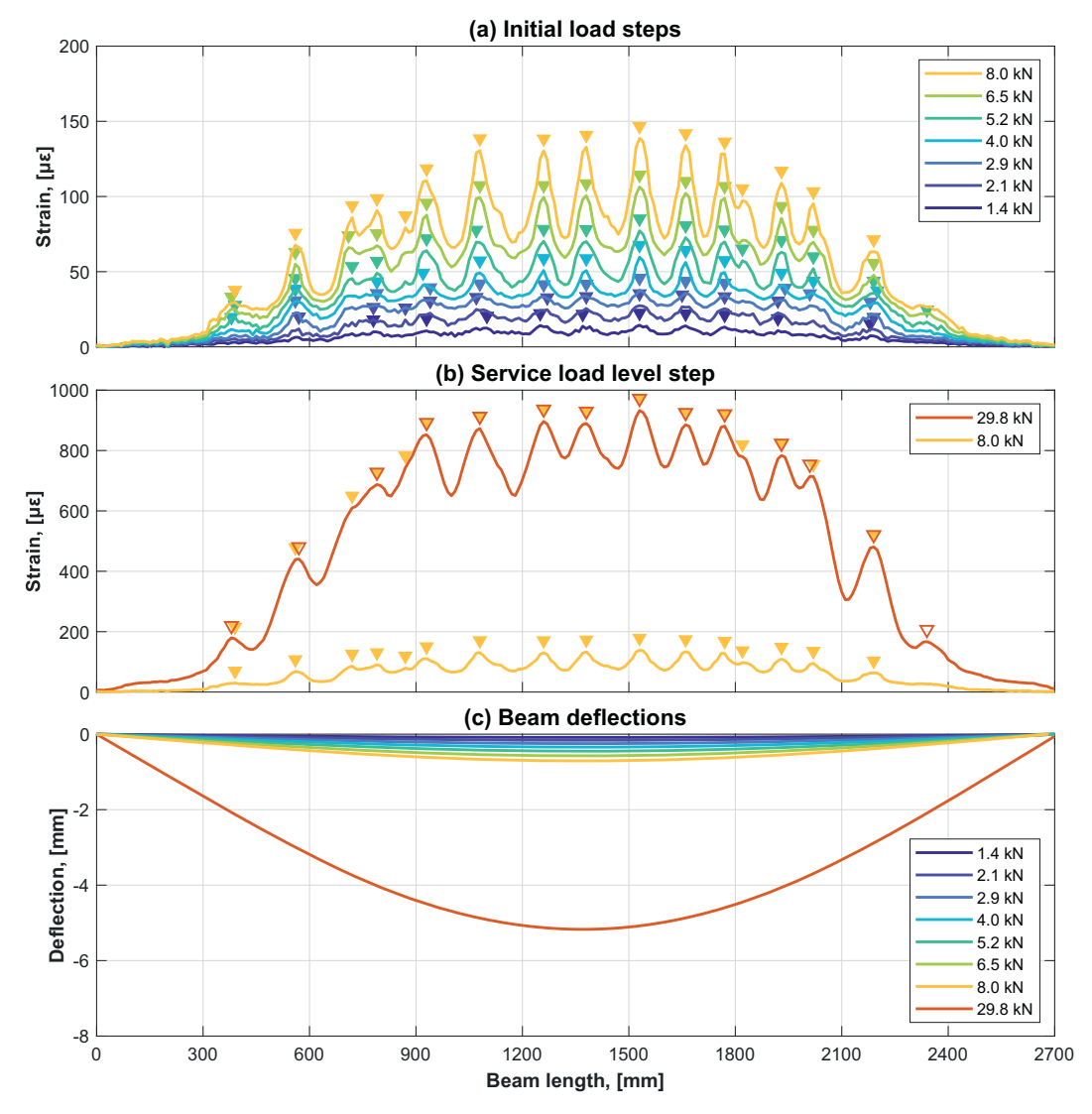


Fig. 13. Experimental measurements for the beam of case study 1. (a) Crack detection based on early strain distribution for different load levels. (b) Comparison of crack detection at low and service load levels. (c) Calculated distribution of deflections for the different load steps.



Fig. 14. Procedure to align the real and virtual beams in the AR tool using two markers.



Fig. 15. Data visualization on the beam through the AR environment after alignment.

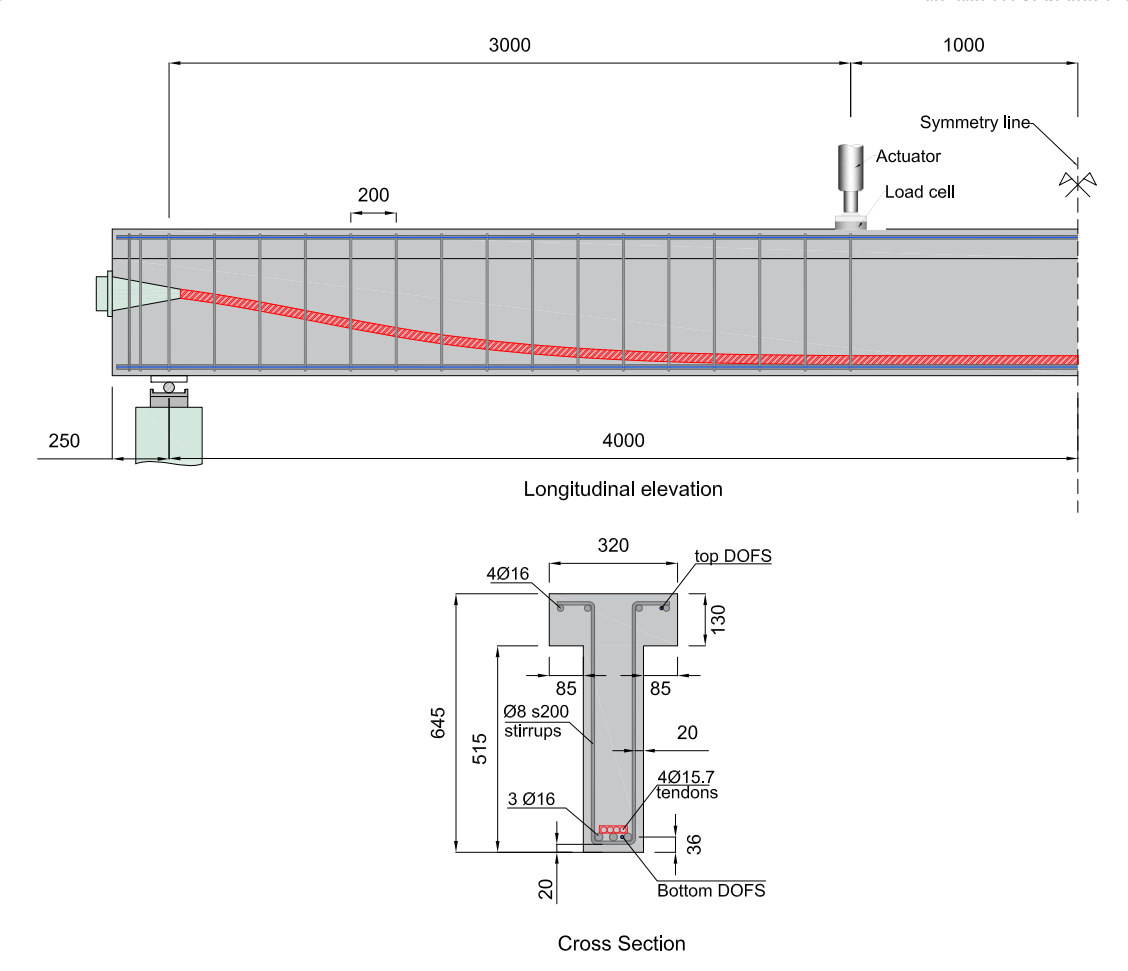


Fig. 16. Geometry, loading setup and DOFS installation configuration for the PRC beam specimen.

utility in visualizing on-site information during inspections. Figs. 19(b) and 19(c) exhibit the strain fields derived from the DOFS sensors at early and advanced load stages, respectively, relative to the failure load. Initial load stages show excellent alignment between the beam and virtual overlay, indicating that the geometry update subroutine effectively adjusts the mesh geometry to convey accurate information to the rendering component. However, at more advanced load stages, some misalignment occurs, not due to inaccuracies in the geometry update subroutine, but because the DOFS occasionally fails to capture viable strain data due to significant local deformations, due to the large discontinuities that cracks represent, potentially leading to non-numeric values (NaN) in the readings. Consequently, the geometry update subroutine, relying on deflection calculations to depict the mesh in its deformed state, may incorporate incorrect data, misrepresenting the actual deflections. This limitation underscores the applicability of DOFS monitoring and AR-enhanced inspections primarily under service loads or conditions not nearing the failure threshold, which aligns with typical inspection protocols. A video demonstrating the system in action during the test is available for further insight.

5. Results and discussion

The results from case study 1 and 2 showed that it was possible to visualize both real-time and historical data through the presented digital twin framework using DOFS, BIM, AR, and the web-based asset inspection system. The laboratory tests demonstrated that these technologies can be merged to support a digital twin framework capable of both on-site and off-site infrastructure health inspections, enabling the analysis and visualization of real-time and historical data. This framework allows for more detailed insights into infrastructure condition and

enhances decision-making through a more data-informed process. As shown in the case studies, the digital twin framework successfully identified and visualized cracks before they became visible to the naked eye, demonstrating the effectiveness of integrating DOFS for early crack detection in combination with AR visualization. This is consistent by Ballor et al. [25] who demonstrated how AR combined with sensorbased structural monitoring improves infrastructure inspection by overlaying critical damage indicators directly onto visual models, enhancing both accuracy and usability in field settings.

Furthermore, the framework enables remote inspection of structural components located in hazardous or hard-to-access environments, thereby reducing the need for on-site presence and improving safety and operational efficiency. When on-site AR was used in the case studies, results showed excellent alignment between the physical and virtual beam overlays. However, the current study was conducted in a controlled laboratory setting. Applying the system in real-world environments with greater variability remains a critical next step. In the lab, QR codes worked well for loading the web-based AR scene and identifying the current location and infrastructure element, but in the field, QR codes must be high-contrast and weather-resistant. While suitable for initialization, they may not be sufficient for spatial tracking and virtual scene anchoring.

In this context, AprilTags QR code-like markers developed for AR tracking could provide more robust spatial tracking when combined with SLAM. In our controlled lab setting, SLAM combined with standard QR codes performed reliably. The performance of AR markers (e.g., QR codes) is influenced by lighting, visibility, and weather. While markers worked reliably indoors, field deployment will require high-contrast, weather-resistant designs or alternatives such as AprilTags for more stable tracking under challenging conditions. However, SLAM systems

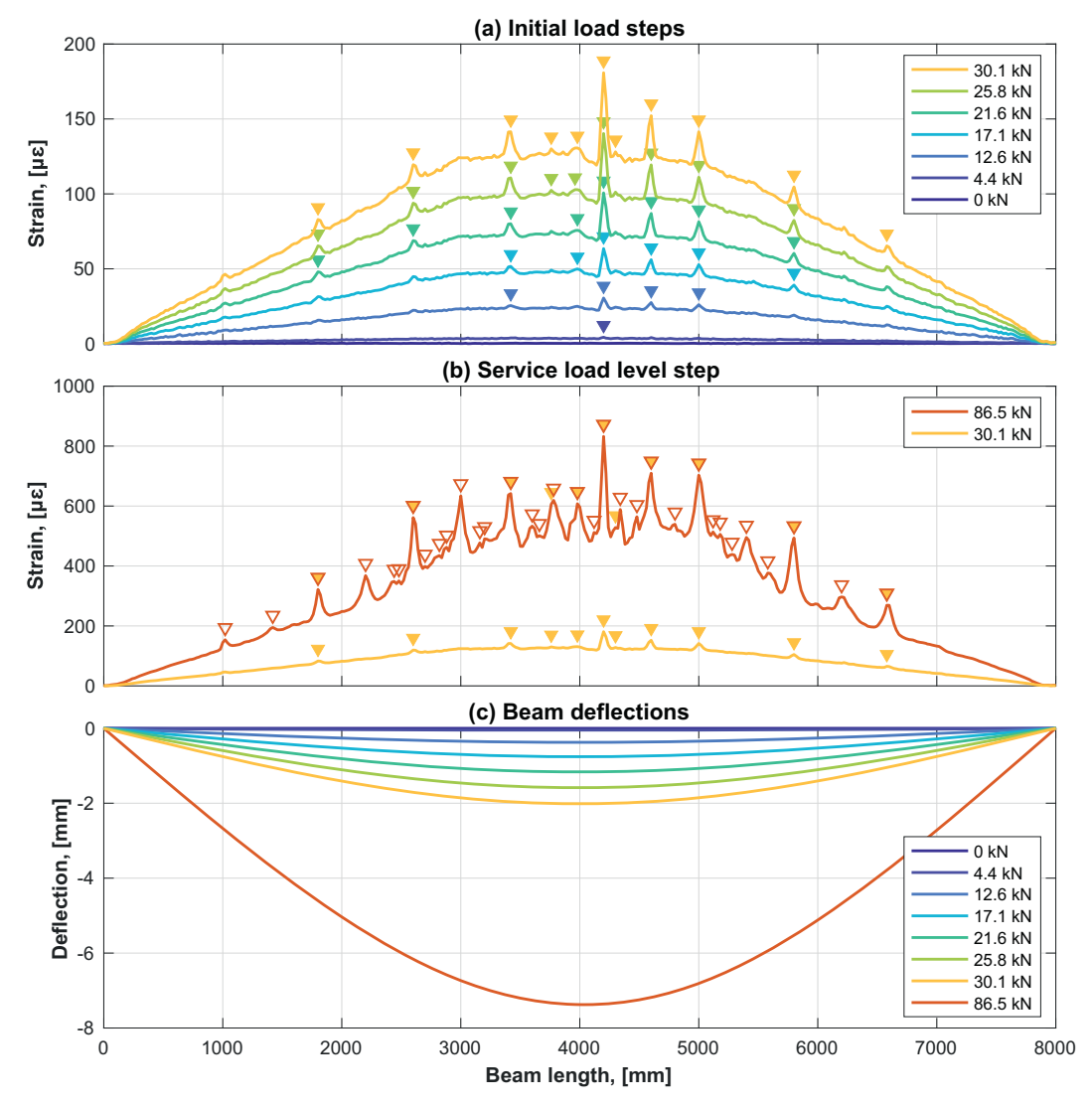


Fig. 17. Experimental measurements for the beam of case study 2. (a) Crack detection based on early strain distribution for different load levels. (b) Comparison of crack detection at low and service load levels. (c) Calculated distribution of deflections for the different load steps.

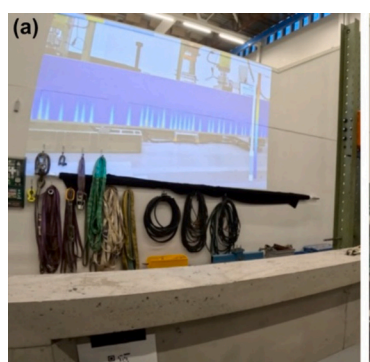
often struggle in low-light, reflective, or textureless environments. Previous studies, including Cadena et al. [26] have shown that maintaining reliable SLAM performance in large-scale or dynamic environments is a significant challenge, reinforcing the need for complementary tracking aids. AprilTags, when used alongside SLAM, have been found to improve pose estimation and tracking efficiency [27]. Additionally, Pfrommer and Daniilidis [28] demonstrated that integrating AprilTags into a SLAM factor graph (TagSLAM) significantly improves pose stability, loop closure, and environmental mapping. In more difficult field conditions

such as large-scale infrastructure with challenging visual features multiple temporary AprilTags or image trackers during inspection may be necessary to accurately anchor and align the virtual and physical scenes. External lighting may also be needed to support tracking in low-light conditions

In some scenarios, location-based tracking using Global Navigation Satellite Systems (GNSS) may be required, particularly for large-scale infrastructure observed from a distance. Wu et al. [29] showed that combining AprilTag detection with Inertial Measurement Units (IMUs)



Fig. 18. (a) Marker position and detection, (b) visualization of the internal components of the beam, i.e. steel reinforcement bars and tendon, and DOFS cables.





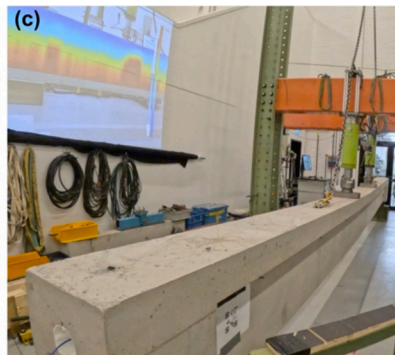


Fig. 19. Real time visualization of postprocessed data within the AR environment. (a) crack withs, (b) and (c) strain fields and early and late load stages respectively.

through visual-inertial fusion provides robust localization even in GNSS-denied environments. The alignment of the AR scene and the validation of marker placement in such real-world scenarios must be further studied before drawing conclusions about the full scalability and robustness of the system. Similar challenges were addressed by Nakaso et al. [30], who developed a hybrid MR system that switches between GNSS-based and marker-based tracking to ensure accurate visualization in both open-sky and obstructed environments. Their findings support the conclusion that real-world applications may require more adaptable spatial anchoring methods such as AprilTags and GNSS beyond standard QR codes and SLAM.

Looking ahead, the deployment of Unmanned Aerial Vehicles (UAVs) in hard-to-access environments could be valuable, especially when combined with DOFS for early-stage crack detection and AR visualization. UAV-assisted crack detection has shown strong potential in field environments. Phung et al. [31] developed an automated UAV inspection system that utilizes image-based crack identification, demonstrating efficiency gains and safety improvements. This highlights the opportunity of integrating UAV-based imaging with DOFS and AR in our framework to identify critical areas for detailed inspection and documentation.

Additionally, the system's interactive interface facilitates real-time visualization of structural parameters such as strain, crack development, and deflections and supports dynamic contour scaling based on user-defined thresholds. A built-in time-history module allows users to examine data evolution through an adjustable time slider. Future research should explore typical threshold values and performance variability across different structural and environmental conditions. Such investigations can provide deeper insight into structural behaviour, load cases, and bearing capacity, both for optimizing design and evaluating the performance of existing structures.

Another practical application of the digital twin framework lies in engineering education, particularly in laboratory settings where students test structural elements such as beams. By integrating DOFS with BIM and AR visualization, the system allows for real-time crack detection and visualization before cracks become visible [32]. This enables students to gain a deeper understanding of material behaviour, structural loading, damage progression, and capacity limits, enhancing their learning through immediate, data-driven feedback during experiments.

Practicality for large-scale civil structures. The proposed framework relies on distributed strain measurements, and it is acknowledged that fully distributed sensing is not feasible at all scales. Nonetheless, current Rayleigh-based OFDR systems enable measurements up to $\sim \! 100$ m per channel with standoff cables of about 200 m, which is already sufficient for many structural elements such as beams, decks, and tunnels. For larger infrastructures, Brillouin-based semi-distributed sensing can extend the sensing range to the kilometer scale, albeit at lower spatial resolution ($\approx \! 200$ mm). This resolution remains sufficient to detect cracks and provide representative strain and deflection fields for inspection purposes. Importantly, the post-processing and visualization

algorithms developed in this work are adaptable across these technologies, ensuring the framework's relevance and scalability to real structures.

Limitations and scope. The proposed reconstruction assumes servicestate behaviour, sufficient bond for strain transfer, and validity of Euler–Bernoulli theory. Near ultimate loads, with large localization, severe slip, or sensor dropout, curvature estimation and mesh warping can degrade; this is consistent with the misalignment observed at advanced load levels in other experiments [5].

6. Conclusions

This paper presented a modular and scalable digital twin framework that integrates Distributed Optical Fiber Sensors (DOFS), Building Information Modelling (BIM), Augmented Reality (AR), and a web-based platform to support infrastructure inspection and structural health monitoring. Through two laboratory case studies, it was demonstrated that the framework enables both real-time and historical visualization of strain, deflection, and crack development offering early-stage damage detection before visual signs are present.

By using cloud-based storage and optimized post-processing, the system enables near real-time overlay of sensor data onto virtual models with minimal latency and low data transfer requirements. The proposed strategy for visualizing deformation using incremental node displacement further reduced computational load, making it suitable for scalable monitoring applications. The integration of AR provided spatially accurate, intuitive visualization of structural performance, supporting remote inspections in potentially hazardous or hard-to-access environments. Unlike traditional digital twin implementations that rely on manual data input, static models, or isolated sensor feedback, the proposed framework offers a real-time, closed-loop integration between high-resolution DOFS data and immersive AR visualization. This synergy allows inspectors to intuitively view strain, crack evolution, and deformation patterns spatially mapped onto actual structures bridging the gap between abstract data interpretation and actionable field understanding. By using lightweight, web-based deployment and minimizing data transmission overhead, the framework also represents a practical and scalable step forward for real-world implementation of sensor-integrated digital twins in construction and infrastructure management.

In addition to field applications, the framework shows potential for engineering education, offering students direct insight into the behaviour of materials and structures through real-time, data-driven experiments. The use of interactive interfaces and time-history modules enables targeted evaluation of the sectional response, steel stresses, sectional curvature and other key parameters in the design process of reinforced concrete structures.

Future research will focus on deploying the framework in large-scale and operational infrastructure to validate performance under variable environmental conditions. This includes the integration of advanced tracking techniques such as AprilTags, GNSS-based localization, and visual-inertial fusion, as well as UAV-assisted inspections for inaccessible assets. Broader application scenarios such as predictive maintenance, digital asset management, and digitally enhanced education will also be explored. However, the authors consider that the framework is practical for real-world applications: current Rayleigh-based DOFS allows spans up to 100 m per channel, and Brillouin-based sensing extends applicability to kilometer-scale infrastructure, albeit at reduced resolution. The developed algorithms are directly adaptable to both technologies, ensuring scalability from laboratory validation to large-scale civil structures.

Overall, this work contributes to the growing body of research on sensor-integrated digital twins and offers a practical pathway toward more informed, safe, and efficient infrastructure inspection workflows in construction and asset management.

CRediT authorship contribution statement

Ignasi Fernandez: Writing – original draft, Visualization, Methodology, Investigation, Conceptualization. Carlos G. Berrocal: Writing – review & editing, Funding acquisition, Data curation. Mikael Johansson: Writing – review & editing, Investigation, Data curation, Conceptualization. Mattias Roupe: Writing – review & editing, Methodology, Conceptualization. Rasmus Rempling: Writing – review & editing, Funding acquisition, Conceptualization.

Funding statement

The present research has been possible thanks to the Smart Build Environment, Swedish funding organization under the grant number 2019–01793.

Declaration of competing interest

The authors declare the following financial interests/personal relationships which may be considered as potential competing interests: Rasmus Rempling reports financial support was provided by Swedish Research Council Formas. If there are other authors, they declare that they have no known competing financial interests or personal relationships that could have appeared to influence the work reported in this paper.

Data availability

Data will be made available on request.

References

- T. Omar, M.L. Nehdi, Data acquisition technologies for construction progress tracking, Autom. Constr. 70 (2016) 143–155, https://doi.org/10.1016/J. AUTCON.2016.06.016.
- [2] I. Fernandez, C.G. Berrocal, R. Rempling, Two-dimensional strain field analysis of reinforced concrete D-regions based on distributed optical fibre sensors, Eng. Struct. 278 (2023), https://doi.org/10.1016/j.engstruct.2022.115562.
- [3] D. Dackman, C.G. Berrocal, R. Rempling, I. Fernandez, A framework for evaluating steel loss from the evolution of corrosion-induced deflections in reinforced concrete beams with non-uniform reinforcement corrosion, Eng. Struct. 317 (2024), https://doi.org/10.1016/J.ENGSTRUCT.2024.118593.
- [4] A. Jansson, A. Sjölander, C.G. Berrocal, R. Rempling, I. Fernandez, Experimental investigation on prevalent local failure mechanisms in hard rock tunnel linings using distributed optical fibre sensors, Eng. Struct. 333 (2025), https://doi.org/ 10.1016/J.ENGSTRUCT.2025.120185.
- [5] I. Fernandez, C.G. Berrocal, S. Almfeldt, R. Rempling, Monitoring of new and existing stainless-steel reinforced concrete structures by clad distributed optical fibre sensing, Struct. Health Monit. 22 (2023) 257–275, https://doi.org/10.1177/ 14752217221081149
- [6] C.G. Berrocal, I. Fernandez, M.F. Bado, J.R. Casas, R. Rempling, Assessment and visualization of performance indicators of reinforced concrete beams by distributed optical fibre sensing, Struct. Health Monit. 20 (2021) 3309–3326, https://doi.org/ 10.1177/1475921720984431.

- [7] D. Agdas, J.A. Rice, J.R. Martinez, I.R. Lasa, Comparison of Visual inspection and structural-health monitoring as bridge condition assessment methods, J. Perform. Constr. Facil. 30 (2015) 04015049, https://doi.org/10.1061/(ASCE)CF.1943-5509.0000802
- [8] Y. Chen, Q. Wang, H. Chen, X. Song, H. Tang, M. Tian, An overview of augmented reality technology, J. Phys. Conf. Ser. 1237 (2019) 022082, https://doi.org/ 10.1088/1742-6596/1237/2/022082.
- [9] Z. Ashour, Z. Shaghaghian, W, Yan, BIMxAR, BIM-Empowered Augmented Reality for Learning Architectural Representations, 2022. http://arxiv.org/abs/2204.032 07. (Accessed 13 June 2025).
- [10] M.O. Adeagbo, S.M. Wang, Y.Q. Ni, Revamping structural health monitoring of advanced rail transit systems: a paradigmatic shift from digital shadows to digital twins, Adv. Eng. Inform. 61 (2024), https://doi.org/10.1016/J.AEI.2024.102450.
- [11] O. Awadallah, A. Sadhu, Automated multiclass structural damage detection and quantification using augmented reality, J. Infrastruct. Intel. Resilience 2 (2023), https://doi.org/10.1016/J.IINTEL.2022.100024.
- [12] C. Brito, N. Alves, L. Magalhaes, M. Guevara, Bim mixed reality tool for the inspection of heritage buildings, ISPRS Annals of the Photogrammetry, Remote Sens. Spatial Informa. Sci. 4 (2019) 25–29, https://doi.org/10.5194/ISPRS-ANNALS-IV-2-W6-25-2019.
- [13] C.S. Park, D.Y. Lee, O.S. Kwon, X. Wang, A framework for proactive construction defect management using BIM, augmented reality and ontology-based data collection template, Autom. Constr. 33 (2013) 61–71, https://doi.org/10.1016/J. AUTCON.2012.09.010.
- [14] H.L. Chi, M.K. Kim, K.Z. Liu, J.P.P. Thedja, J. Seo, D.E. Lee, Rebar inspection integrating augmented reality and laser scanning, Autom. Constr. 136 (2022) 104183, https://doi.org/10.1016/J.AUTCON.2022.104183.
- [15] Y. Zhou, H. Luo, Y. Yang, Implementation of augmented reality for segment displacement inspection during tunneling construction, Autom. Constr. 82 (2017) 112–121, https://doi.org/10.1016/J.AUTCON.2017.02.007.
- [16] J.M. Huang, S.K. Ong, A.Y.C. Nee, Visualization and interaction of finite element analysis in augmented reality, Comput. Aided Des. 84 (2017) 1–14, https://doi. org/10.1016/J.CAD.2016.10.004.
- [17] D.C. Nguyen, T.Q. Nguyen, R. Jin, C.H. Jeon, C.S. Shim, BIM-based mixed-reality application for bridge inspection and maintenance, Constr. Innov. 22 (2022) 487–503, https://doi.org/10.1108/CI-04-2021-0069.
- [18] D. Liu, X. Xia, J. Chen, S. Li, Integrating building information model and augmented reality for drone-based building inspection, J. Comput. Civ. Eng. 35 (2020) 04020073, https://doi.org/10.1061/(ASCE)CP.1943-5487.0000958.
- [19] I. Fernandez, C.G. Berrocal, R. Rempling, Long-term performance of distributed optical fiber sensors embedded in reinforced concrete beams under sustained deflection and cyclic loading, Sensors 21 (2021), https://doi.org/10.3390/ \$21166338
- [20] M. Li, X. Feng, Y. Han, Brillouin fiber optic sensors and mobile augmented reality-based digital twins for quantitative safety assessment of underground pipelines, Autom. Constr. 144 (2022) 104617, https://doi.org/10.1016/J. AUTCON.2022.104617.
- [21] Alan R. Hevner, A three cycle view of design science research, Scand. J. Inf. Syst. 19 (2) (2007). Article 4. Available at: https://aisel.aisnet.org/sjis/vol19/iss2/4.
- [22] A.R. Hevner, S.T. March, J. Park, S. Ram, Design science in information systems research, MIS Q. 28 (2004) 75–105, https://doi.org/10.2307/25148625.
- [23] C.G. Berrocal, I. Fernandez, R. Rempling, Crack monitoring in reinforced concrete beams by distributed optical fiber sensors, Struct. Infrastruct. Eng. 17 (2021) 124–139, https://doi.org/10.1080/15732479.2020.1731558.
- [24] I. Fernandez, D. Ekström, R. Rempling, C.G. Berrocal, Evaluation of post-tensioned reinforced and fiber reinforced concrete beams by using DOFS, Struct. Concr. (2025), https://doi.org/10.1002/SUCO.70224.
- [25] D.D.L. Mascareñas, J.A.P. Ballor, O.L. McClain, M.A. Mellor, C.Y. Shen, B. Bleck, J. Morales, L.M.R. Yeong, B. Narushof, P. Shelton, E. Martinez, Y. Yang, A. Cattaneo, T.A. Harden, F. Moreu, Augmented reality for next generation infrastructure inspections, Struct. Health Monit. 20 (2021) 1957–1979, https://doi.org/10.1177/1475921720953846.
- [26] C. Cadena, L. Carlone, H. Carrillo, Y. Latif, D. Scaramuzza, J. Neira, I. Reid, J. J. Leonard, Past, present, and future of simultaneous localization and mapping: toward the robust-perception age, IEEE Trans. Robot. 32 (2016) 1309–1332, https://doi.org/10.1109/TRO.2016.2624754.
- [27] S.M. Abbas, S. Aslam, K. Berns, A. Muhammad, Analysis and improvements in apriltag based state estimation, Sensors 19 (2019) 5480, https://doi.org/10.3390/ S19245480.
- [28] B. Pfrommer, K. Daniilidis, TagSLAM: Robust SLAM with Fiducial Markers. htt ps://arxiv.org/pdf/1910.00679, 2019 accessed August 4, 2025.
- [29] Z. Wu, H. An, B. Wu, H. Wang, K. Lu, A. Visual-Inertial Fusion Mapping, Localization System Using AprilTag in GNSS-Denied Scenes, Lecture Notes in Computer Science (Including Subseries Lecture Notes in Artificial Intelligence and Lecture Notes in Bioinformatics) 14275 LNAI, 2023, pp. 261–272, https://doi.org/ 10.1007/978-981-99-6504-5 23.
- [30] R.N. Nakaso, K.K. Kashiyama, T.K. Kotoura, Development of a Mixed Reality visualization system using a location-based method for the underwater objects, in: 16th World Congress on Computational Mechanics and 4th Pan American Congress on Computational Mechanics, 2024, https://doi.org/10.23967/WCCM.2024.108.
- [31] M.D. Phung, T.H. Dinh, V.T. Hoang, Q.P. Ha, Automatic crack detection in built infrastructure using unmanned aerial vehicles, in: ISARC 2017 - Proceedings of the

- 34th International Symposium on Automation and Robotics in Construction, 2017, pp. 823–829. https://doi.org/10.22260/ISARC2017/0115
- pp. 823–829, https://doi.org/10.22260/ISARC2017/0115.
 [32] I. Fernandez, C.G. Berrocal, R. Rempling, Making the invisible visible: augmented reality and distributed optic Fiber in educational structural engineering labs, in: Tenth International Conference on Higher Education Advances, 2024, https://doi.org/10.4995/HEAd24.2024.17142.
- [33] A.C.P. Martins, I.R. Castellano, K.M. Lenz César Júnior, J.M. Franco de Carvalho, F. G. Bellon, D.S. de Oliveira, J.C.L. Ribeiro, BIM-based mixed reality application for bridge inspection, Autom. Constr. 168 (2024) 105775, https://doi.org/10.1016/J. AUTCON.2024.105775.